Ahmad Paknejad[1]
BEAMS Department,
Université Libre de Bruxelles,
Brussels 1050, Belgium
e-mail: ahmad.paknejad@ulb.be

Rasa Jamshidi
BEAMS Department,
Université Libre de Bruxelles,
Brussels 1050, Belgium;
Aerospace and Mechanical Engineering
Department,
Université de Liège,
Liège 4000, Belgium

Shashank Pathak
BEAMS Department,
Université Libre de Bruxelles,
Brussels 1050, Belgium;
School of Civil & Environmental Engineering,
Indian Institute of Technology,
Mandi, Himachal Pradesh 175075, India

Christophe Collette
BEAMS Department,
Université Libre de Bruxelles,
Brussels 1050, Belgium;
Aerospace and Mechanical Engineering
Department,
Université de Liège,
Liège 4000, Belgium

Active Vibration Mitigation of Bladed Structures With Piezoelectric Patches by Decentralized Positive Position Feedback Controller

This paper proposes an active damping system to mitigate the vibration of bladed assemblies. The damping system consists of multiple pairs of piezoelectric patches accompanied by a decentralized control configuration. To maximize the control authority, the size and the location of the patches are optimized based on maximizing the strain energy. In each pair, one patch is used as a sensor and the other one as an actuator. As the control plants of such configuration have no high-frequency roll-off, a second-order low-pass filter known as a positive position feedback (PPF) controller is considered as the control law. The parameters of the controller are tuned based on maximizing the closed-loop damping of the first family of modes. This active damping system is implemented on a monobloc bladed rail which is representative of a portion of bladed drum, i.e., BluM. Numerical simulations are performed to assess the performance of the designed control system and experimental tests are carried out to validate the numerical design.
[DOI: 10.1115/1.4056013]

Keywords: active vibration control, lightly damped structures, smart structures, turbomachinary

1 Introduction

Current trends in turbomachinery applications for achieving higher functional efficiency with lower energy consumption have led to several changes in the design of bladed assemblies. One of the main ideas is to reduce the centrifugal loads applied to the bladed structures. This can be done by lowering the total mass using new materials, lightweight structural design, or a new fabrication technique. For example, manufacturing the blades on a drum-like support in a single piece, i.e., BluM can provide a mass reduction compared to a classical design where the blades were attached to the support using fixing solutions. This solution however comes at the price of a very low structural damping leading to high amplitude vibrations as the blades are subjected to aerodynamic excitations. An undesirable consequence of this behavior is to drastically increase the noise propagation and reduce the lifespan of the structure because of high cycle fatigue. To solve the issue, a vibration-damping device needs to be integrated into the structures. One of the well-known technique is the friction damping [1]. As friction dampers are nonlinear systems [2,3], the damping performance depends on the level of relative motions and the contact area between the parts [4]. A special attention to the use of piezoelectric transducers has been given to bladed structures because of lightweight components added into structures. There are two common vibration control systems known as passive and active.

Passive control systems are simply integrated into the structures with no need for external power sources and additional hardware for their operations. Piezoelectric patches connected to an electrical network known as shunt damping is a promising technique to mitigate the vibration of bladed structures. Basically, the piezoelectric effect transforms mechanical energy into electrical energy which is dissipated through the electrical network [5]. Schwarzendahl et al. [6] implemented this technique on a bladed structure and optimized the parameters of the shunt to minimize the amplitude of the first mode. Mokrani et al. [7] tuned the shunt elements using the average frequency of the first bending modes family. Although the passive shunt is an interesting vibration damping system, its performance is strongly dependent on the electromechanical coupling factor [8].

Active control systems were introduced to overcome the performance limitations of the passive methods since they are less sensitive to the system's parameters [9]. They however require external energy source for their operations. The use of such techniques in order to improve the control authority of the piezoelectric shunt damping was studied on the bladed structures. Kauffman et al. [10] proposed a semi-active approach using low-power frequency-switching. The use of negative capacitance was proposed in Ref. [8] and implemented on a test-rig of a bladed disk model with eight blades [11]. Note that the negative capacitance is an active electrical device. Tang et al. [12] implemented an active-passive-hybrid-piezoelectric-network (known as APPN), which was initially introduced by Agnes [13], on a rotationally periodic structure. Basically, APPN integrates piezoelectric shunt damping with an active voltage or charge source to improve the performance of the system.

In addition, active control systems can be applied by integrating sensors, actuators, and control units. Despite the potential of such systems, only a few studies have focused on using such tools for bladed structures. An active control system has been implemented on general electric aviation subscale composite fan blades using piezoelectric patches as sensors and actuators. In this study [14], the control system has been inspired by the transfer function of a simple resistive-inductive circuit which is used for the passive

piezoelectric shunt damping. It has been reported that the advantages of this technique compared to the common passive technique are the use of an amplifier to achieve a higher actuation level and the fact that the active control does not require an actual resistor or inductor, which can be very large-sized at low target frequencies. A number of studies have proposed active noise control to reduce the source of engine noise induced by the large fan at the front of the engine of modern commercial jet aircraft [15–18]. For example, an active noise control system, designed in Ref. [19], consists of multiple microphones as sensors, multiple piezoelectric patches as actuators, and adaptive filters for controlling unit.

When piezoelectric sensor and actuator are collocated, the open-loop transfer function contains an alternating pole-zero configuration which has no high frequency roll-off. Depending on the strain distribution of a mode at the location of the piezoelectric patches, the zero of the open-loop transfer function may appear either after or before the pole. This is an important key in the design of the active control system. When the zero comes after pole, positive-position-feedback (PPF) is proposed as an interesting active control law. Although it amplifies the static response which may lead to a decrease in the stiffness of the structure, the controller adds the high-frequency roll-off. PPF can be implemented by using a first- or a second-order filter. The second-order PPF outperforms the first-order PPF in terms of the damping ratio of a target mode; however, its performance degrades rapidly under the resonance uncertainty. This technique was implemented on a cantilever beam when its parameters were optimized based on the method of maximum damping [20] and H∞ optimization [21].

This work aims to evaluate the performance of second-order PPF to damp the vibration of bladed structures. In particular, the focus is on the monobloc bladed rail, which represents a section of the bladed drum, i.e., BluM. Section 2 provides a finite element model of the structure. This section also includes the optimal location of the piezoelectric patches. The control system is designed in Sec. 3 and its performance is assessed numerically. Afterward in Sec. 4, an experimental test is carried out to validate the proposed controller performance on mitigating the resonances of the first modes family. During the operation of the BluM, there are some energetic orders which excite significantly the first family. This is why we focus on this family. The conclusions are drawn in Sec. 5.

2 System Under Consideration

In Ref. [7], the dynamics of bladed drum known as BluM have been studied. The BluM is a part of the low-pressure stage of the compressor of a jet engine designed by Safran. It has been highlighted that one of the main dynamic behavior of the BluM is high modal density resonances. The high modal density resonances are caused by the resonances of the blades present in a narrow frequency range. The challenge is to design a vibration damping system that considers all the resonances. There are 72 blades on the BluM. Modeling and verifying any vibration damping system on the BluM would be a big step. In this study, we focus on a simplified bladed structure, called bladed rail, representing a portion of the BluM with five blades. In Sec. 2.1, we first study the dynamic behavior of the bladed rail to ensure that the trend of the dynamic behavior is the same as the main application, i.e., the BluM.

2.1 Numerical Modeling of the Bladed Rail. The BluM is made of titanium and the blades are attached to the support using friction welding. Figure 1 shows the manufactured bladed rail using three-dimensional printing and aluminum material properties. Note that different material properties and manufacturing process may move the resonances to slightly a lower or higher frequency, while it is assumed they do not change the mode shape, qualitatively. The monobloc bladed rail comprises five identical blades placed on a support. The size and geometry of the blades are adapted to that of the conventional BluM [7]. As a boundary
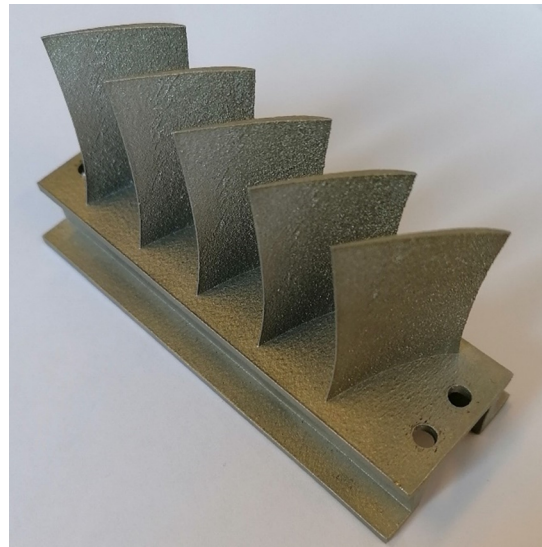

Fig. 1 The bladed rail

condition, the two ends of the structure are clamped to rigid supports using the two holes on each side. The rigid supports are made of steel with natural frequencies much higher than the resonances of first family. In addition, the thickness and the cross section of the support are the same as that of the BluM. Therefore, the support of the bladed rail is stiffer than that of the BluM. Although higher stiffness of the support puts the resonances of the blades closer to each other, it is assumed that the mode shapes of blade resonances remain the same qualitatively.

Due to the complexity of the structure, the bladed rail has been modeled based on the finite element method as shown in Fig. 2(a). The model has been made of two-dimensional shell elements in structural dynamic toolbox in MATLAB. The normalized frequencies of the first twenty modes of the structure are shown in Fig. 2(b). Note that the frequencies are normalized with respect to the frequency of the first resonance. Clearly, modes can be categorized into two types. The first type corresponds to the mode family consisting of five resonances with very close frequencies. These resonances correspond to the blade modes where the blades vibrate according to one of their cantilever mode shapes as shown in Fig. 3. Therefore, the maximum motion appears at the blades for such resonances, while the support is almost motionless. The mode shapes of the first resonance of the first three families are presented in Fig. 3. It can be seen that the first, second, and third families are related to the first bending, first torsion, and second bending of the cantilever blades, respectively. For all resonances in each family, the blades experience the same cantilever mode shape although they can move in-phase or out-of-phase with respect to the ones in their neighborhood with different amplitude of motion. This is the consequence of the flexible support. If the support was infinitely rigid and the blades were exactly identical, the resonances of a family would have the same frequency and shape. In addition, the second type of resonances, isolated from others in Fig. 2(b), represents the modes of the support. In this case, the blades have only translational motion caused by the deformation of the support. In this study, the vibration of the first family of modes is of interest.

2.2 Optimal Location of Piezoelectric Patches. Piezoelectric materials transform mechanical energy into electrical energy and vice versa. This property allows us to use them as either sensors and/or actuators. When a piezoelectric patch is used as a sensor, the output voltage or charge is proportional to the sum of mechanical strains experienced by the patch. In the case of actuation, the piezoelectric patch induces a moment of force equivalent
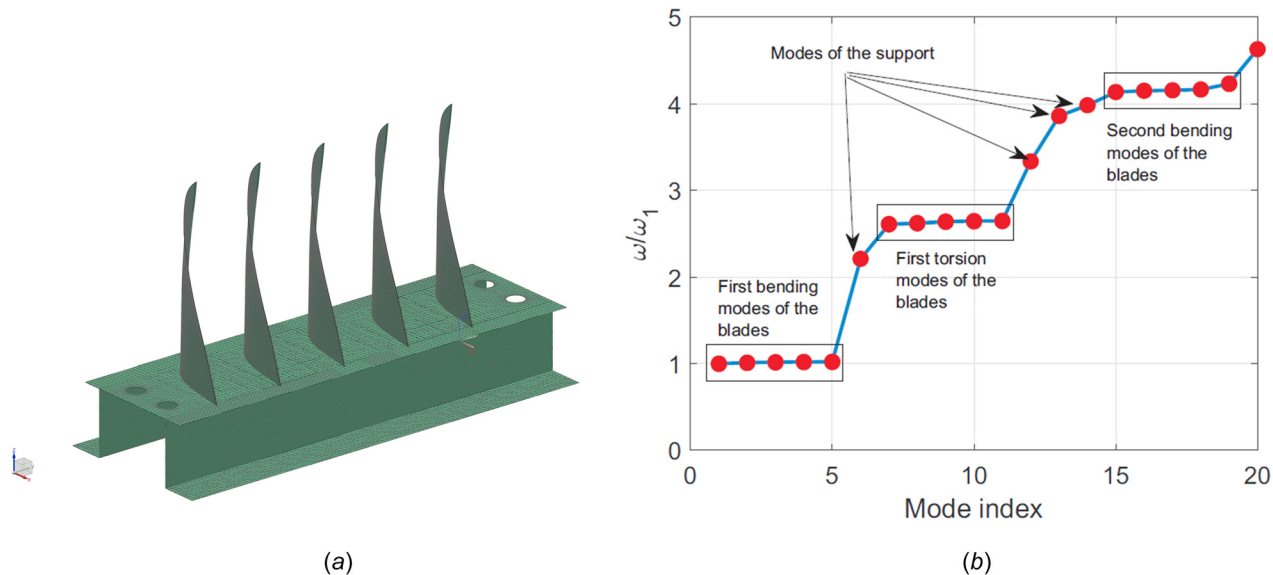
(a)　　　　　　　　　　　　　　(b)

Fig. 2 **(a) Model of the bladed rail structure and (b) normalized resonance frequencies of the bladed assemblies (ω1 is the first bending mode frequency of the first family)**
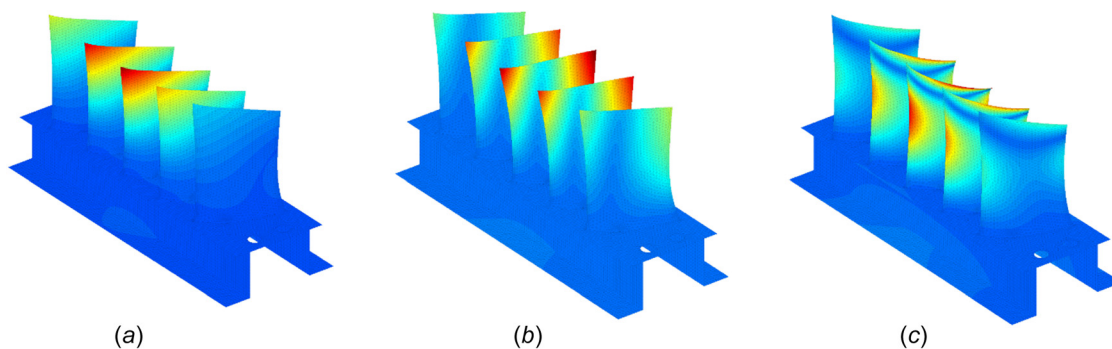

(a)　　　　　　　　　(b)　　　　　　　　　(c)

Fig. 3 **Mode shapes of (a) the first resonance of the first family, (b) the first resonance of the second family, and (c) the first resonance of the third family**

to a stress/strain distribution, which is proportional to the applied voltage. Therefore, to maximize the observability and controllability, the optimal location of these transducers is the area of the structure where the strain energy is maximized. The strain energy map of the first five modes corresponding to the first family of modes is illustrated in Fig. 4. One sees that the strain energy is maximized close to the root of each blades. However, patches cannot be placed there, because they can easily disturb the aerodynamic flow around the blades. To overcome the aforementioned limitation, it is required to place the transducers on the internal part of the rail. For this area, the strain energy map is shown in Fig. 5(a). It is clearly visible that a local strain distribution is generated inside the support below the base of each blade. The local deformations are separated by an artificial nodal line (highlighted by gray dashed lines) where no strain is generated. Depending on the motion of a blade, the deformation is either in tension or in compression; and subsequently, the charge generated in a piezoelectric patch is either positive or negative. In order to avoid charge cancelation in the patches, the size of piezoelectric patches cannot be greater than the local deformation area.

It should be noted that as the local deformations are caused by the motion of the blades while the support is not involved globally, it is assumed that similar dynamic behavior is present on the real application, i.e., BluM.

The key point to applying highly stable active control law is to choose a collocated open-loop transfer function. The collocated system means that the frequency response function (FRF) from

voltage applied by the actuator to the voltage measured by the sensor contains alternating pole and zero. In this configuration, the phase remains always bounded between 0 deg and ±180 deg allowing high stability margin in the closed-loop system. This can be done by placing the piezoelectric sensor and actuator at a location where they share the same sign of modal strain. Consequently, one pair of piezoelectric patches is placed inside the support below the base of each blade at the local strain map as can be seen in Fig. 5(b).

The strain energy map shown in Figs. 4 and 5 contains the average of the strain energy in all directions and does include the sign of the strains. In addition, those strain energy maps are presented without the piezoelectric patches. To evaluate the strain maps in different directions and the effect of the piezoelectric patches on the strain distribution, Fig. 6 shows the strain maps corresponding to the third mode of the first family in the first two directions. Note that five pairs of PIC155 patches are modeled. The material properties of the patches are given in Ref. [22]. Although the strain maps are shown for one mode, the same conclusions can be made for other modes as well. As the thickness of the patches is smaller with respect to other two dimensions, the impact of the strain in the third direction on the charge of the piezoelectric patches is negligible. According to Fig. 6, the following conclusions can be made:

● Considering a local deformation, the sign of strain in both directions is the same and is fixed. Therefore, the local
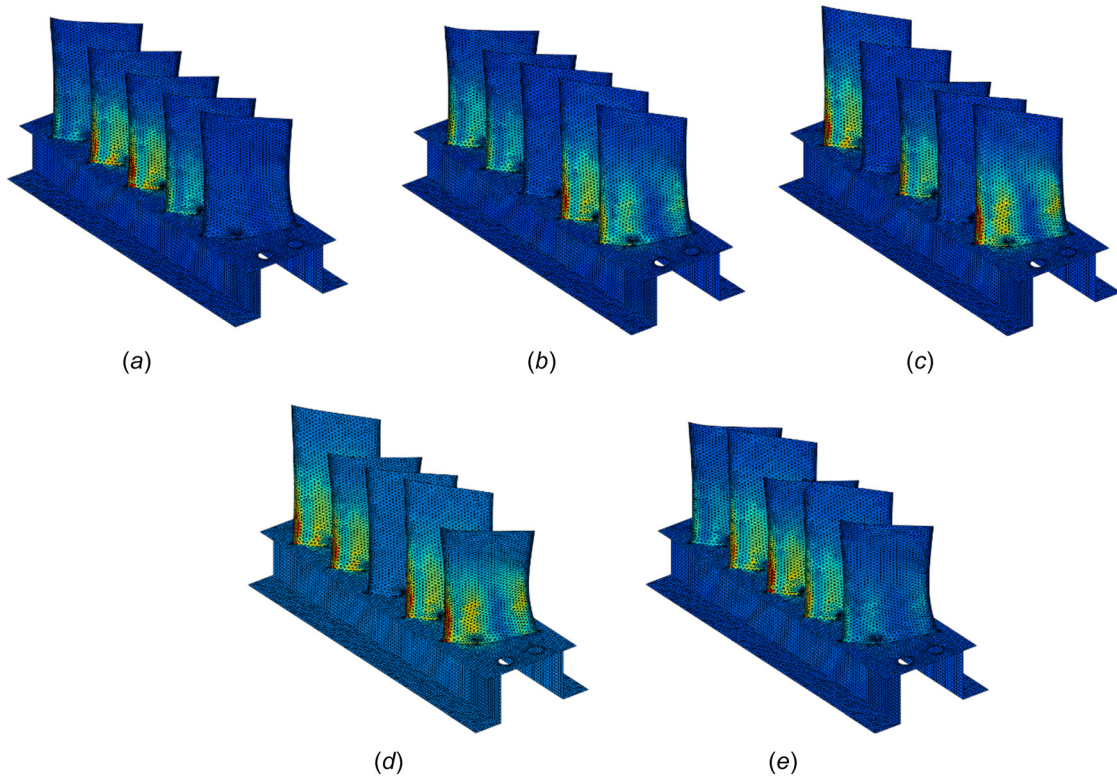
Fig. 4 Strain energy map of the first family of modes: (*a*) first mode, (*b*) second mode, (*c*) third mode, (*d*) fourth mode, and (*e*) fifth mode
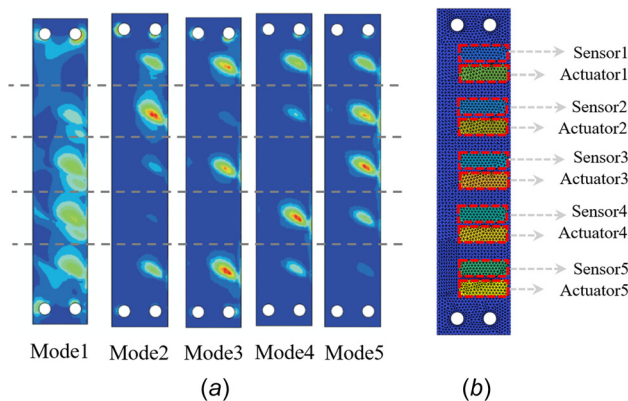

Fig. 5 (*a*) Strain energy map of the internal part of the support for the first family of modes and (*b*) configuration of the piezoelectric patches on the structure

deformation is either in tension or compression for both directions. This ensures that the charge of both patches in one pair has the same sign.

- The mass and stiffness of the patches do not disarrange the strain map of a local deformation, qualitatively.

3 Control Design

The open-loop transfer function from each piezoelectric actuator Va_i to its collocated piezoelectric sensor Vs_i is shown in Fig. 6. One sees that the system contains alternating pole-zero configuration with no high frequency roll-off. For each mode, the frequency of the pole is the same for all pairs because it corresponds to a resonance frequency of the blades, while the frequency of the zero changes. In an active control system, the controllability of a target mode can be assessed by the frequency difference between its pole and its zero. In fact, the highest frequency difference will provide the highest control ability. When the zero of a mode is
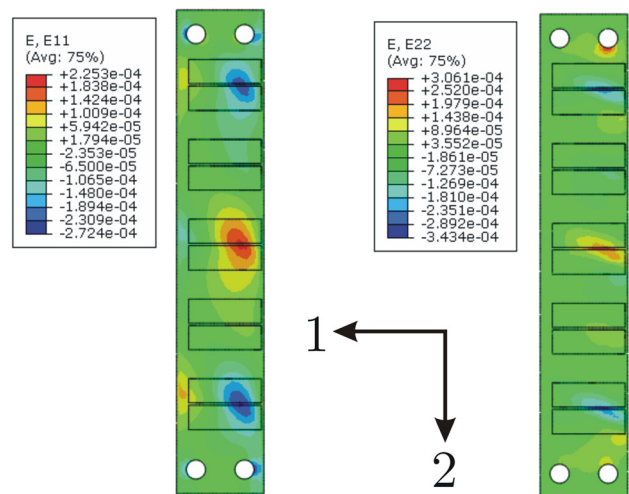

Fig. 6 Strain map in the first direction (the left figure) and the second direction (the right figure)

placed so close to its pole, not only there is no controllability of that mode, but also the mode cannot be clearly observed in the open-loop response. For example, the fourth mode cannot be observed from the open-loop response of the third loop as shown in Fig. 7. As a result, the third, the second, the first, the fifth, and the fourth loops are employed in this study to target the first, the second, the third, the fourth, and the fifth modes, respectively. Note that there is no unique solution to the selection of the loops. As each loop targets one resonance, there will be five decentralized control laws as shown in Fig. 8.

The choice of the control law is dependent on the location of zeroes with respect to poles in the open-loop transfer function. It has been shown that the second-order filter known as the positive
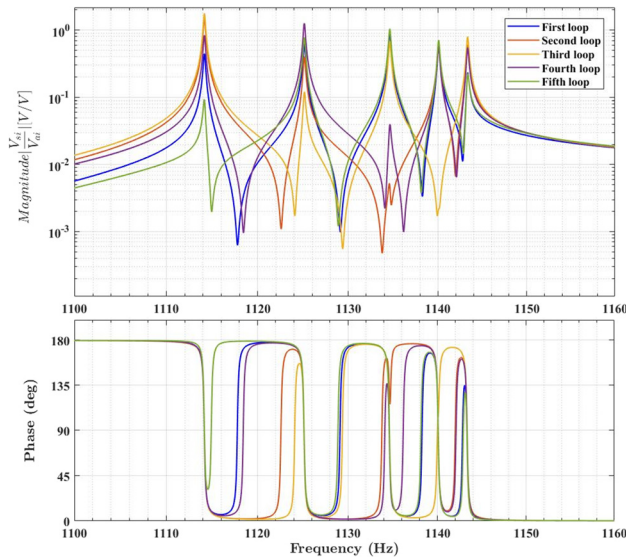
Fig. 7 FRF of the open-loop transfer function from each piezoelectric actuator to its collocated piezoelectric sensor

position feedback (PPF) is an effective control laws when the open-loop transfer function starts with a pole. A novel method for determining the constants of the PPF controller proposed by Paknejad [16] is used in this study. The controller aims to target ith resonance with a modal stiffness k_i and the resonance frequency ω_i. Therefore, targeting the ith mode of the structure, the control law is given by

$$G_i(s) = + \frac{g_{f_i} \omega_{f_i}^2}{s^2 + 2\xi_{f_i} \omega_{f_i} s + \omega_{f_i}^2} \qquad (1)$$

where ω_{f_i}, ξ_{f_i}, and g_{f_i} are the tuning frequency of the controller, the damping ratio of the controller, and the feedback gain. These parameters can be found as follow [16]:

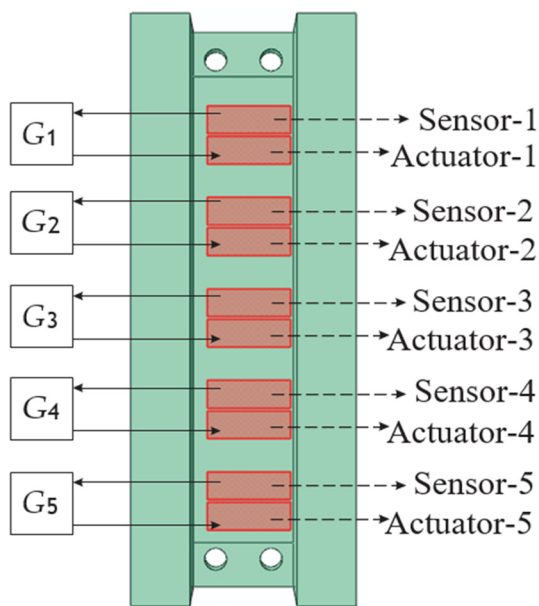$$\omega_{f_i} = \omega_i \sqrt{4\eta_i^2 + 1} \qquad (2a)$$

Fig. 8 Configuration of the piezoelectric patches for the implementation of the active control system

$$g_{f_i} = \frac{4\eta_i^2 k_i}{4\eta_i^2 + 1} \qquad (2b)$$

$$\xi_{f_i} = \frac{2\eta_i}{\sqrt{4\eta_i^2 + 1}} \qquad (2c)$$

where η is the desired damping of closed-loop poles. For the numerical simulations, the modal stiffness is obtained based on the orthogonality conditions. For this purpose, a numerical modal analysis is performed using structural dynamic toolbox to extract the resonance frequencies, the modal mass matrix, and mode shapes [23]. Knowing the modal mass and the resonances, the modal stiffness matrix is obtained. The optimal parameters of the PPF for each loop are listed in Table 1. In the last column of the table, it is indicated which loop targets which mode. This choice is made based on the distance between the frequency of pole and zero. In active control system, the controllability of a target resonance can be assessed by the distance between the frequency of the pole and the frequency of the zero. Table 2 shows the distance between the frequency pole and zero. The selected loop for each mode is highlighted in yellow color. The selection of the loops is not unique. One can choose other loops.

Before all the loops are closed at the same time, the performance of the PPF is evaluated on each loop as a single input single output. The loop gains for all loops are presented in Fig. 9. The loop gain is defined as the multiplication of the open-loop transfer function to the corresponding PPF controller. One sees that the system is stable for all individual loops with minimum 45 deg phase margin. Note that the highest loop gain for each loop appears at the corresponding target mode. In addition, the FRF of the open-loop transfer function for the first loop is compared to that of the closed-loop in Fig. 10. Interestingly, the designed PPF can considerably damp the third mode. Moreover, the controller is also effective in the other modes. Figure 10 is just an example to indicate the performance of PPF on the target mode and the other modes. Similar conclusions can be made on the other loops.

The aim of the designed control system is to reduce the vibration of the blades around at resonance frequencies of the first family. Therefore, the performance index of the system is defined by a transfer function from an excitation force at the tip of the middle blade to the displacement at the same location. Figure 11 shows the FRF of the performance index without the control system and with the control system when all loops are closed. Similar to the real application, the modal damping ratio of the primary system is 0.01%. Therefore, it can be seen that amplitudes of the closed-loop response reduced at least 10 times lower than those of the primary system.

4 Experimental Test

In this section, an experimental setup is carried out for validating the decentralized PPF controller on the bladed rail designed in Sec. 3. For this purpose, the bladed rail structure has been manufactured with aluminum material. Then, five pairs of piezoelectric patches have been glued at the optimal locations mentioned previously in Fig. 5(b). Also, two supports have been used to clamp the structure from both ends. The supports have been designed rigid enough with a first resonance frequency far from the resonances

Table 1 Designed PPF controller parameters for each loop

Loops	ω_f (Hz)	ξ_f (%)	g_f	η_i (%)	k_i (N/m)	Target mode
1	1137.5	7.18	1.7517×10^8	3.6	9.03×10^5	Third
2	1128.0	7.18	1.6653×10^8	3.6	8.59×10^5	Second
3	1117.2	7.18	1.6128×10^8	3.6	8.32×10^5	First
4	1146.3	7.18	2.6009×10^8	3.6	1.34×10^6	Fifth
5	1143.0	7.18	2.2924×10^8	3.6	1.18×10^6	Fourth

Table 2 Frequencies of pole and zeroes for each mode of the family

| Parameter		Mode 1 (Hz)	Mode 2 (Hz)	Mode 3 (Hz)	Mode 4 (Hz)	Mode 5 (Hz)
Loop 1	Poles	1114.1	1125.1	1134.6	1140.1	1143.4
	Zeroes	1117.8	1129.1	1138.3	1142.8	n/a
	Difference	3.7	4	3.7	2.7	n/a
Loop 2	Poles	1114.1	1125.1	1134.6	1140.1	1143.4
	Zeroes	1122.6	1133.8	1134.8	1142	n/a
	Difference	8.5	8.7	0.2	1.9	n/a
Loop 3	Poles	1114.1	1125.1	1134.6	1140.1	1143.4
	Zeroes	1124.1	1129.4	1139.9	1140.2	n/a
	Difference	10	4.3	5.3	0.1	n/a
Loop 4	Poles	1114.1	1125.1	1134.6	1140.1	1143.4
	Zeroes	1118.4	1134.1	1136.2	1142.1	n/a
	Difference	4.3	9	1.6	2	n/a
Loop 5	Poles	1114.1	1125.1	1134.6	1140.1	1143.4
	Zeroes	1114.9	1128.9	1138.1	1142.9	n/a
	Difference	0.8	3.8	3.5	2.8	n/a
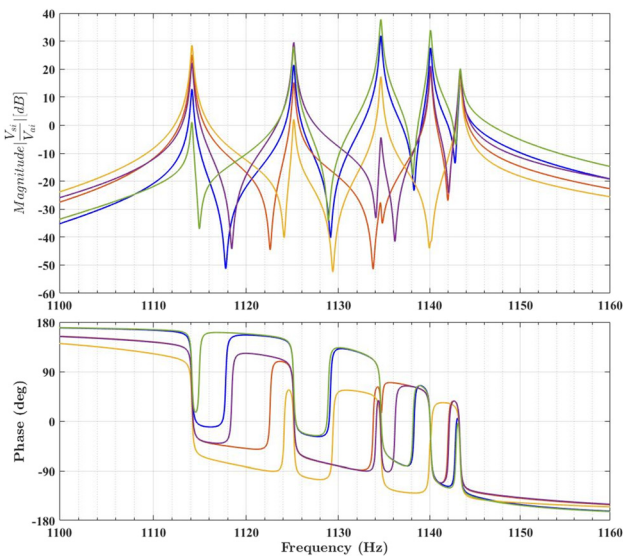
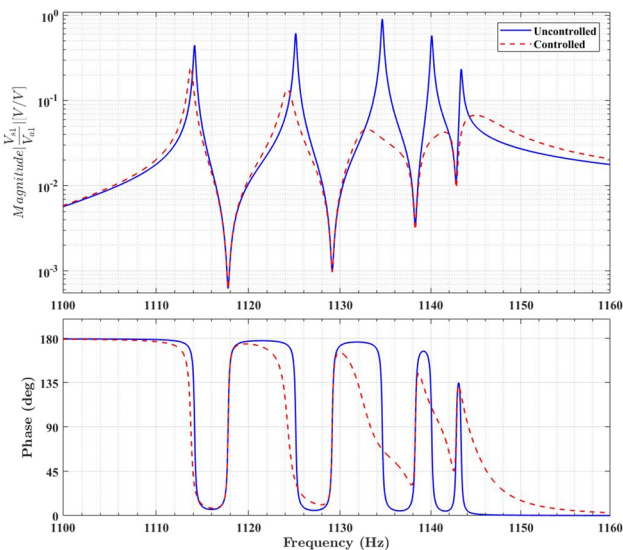
Fig. 9 Numerical FRFs of the loops gains

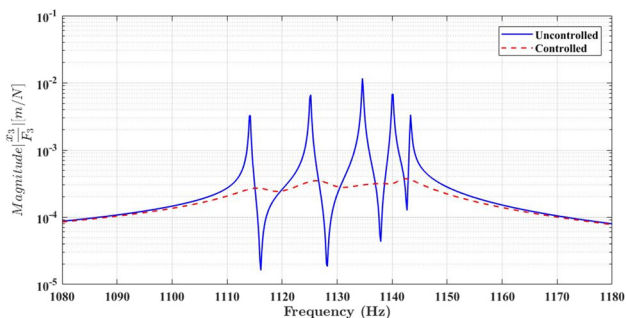Fig. 10 Open loop and closed loop response of loop no. 1

Fig. 11 Performance index of the bladed rail (the transfer function between the middle blade's force to the middle blade's tip displacement) in controlled and uncontrolled condition

of the first family. The pictures of the experimental setup are presented in Fig. 12.

To perform the experimental tests, a DSPACE MICRO-LABBOX was used for the purpose of both the data acquisition and the control system. The control configuration is designed first inside the graphical SIMULINK environment of MATLAB and then compiled. The compiled file is uploaded into the CONTROLDESK software connected directly to the MICRO-LABBOX hardware. The system is running in real-time at a sampling frequency of 20 kHz. The measured data were also recorded at the same sampling frequency. It is interesting to note that such practical implementation of the active control system is only used to verify the design on the laboratory scale. This method cannot be used for real application, i.e., BluM. On the other hand, as the PPF is a resonator, it is possible to realize it by means of an analog electric circuit using operational amplifier. The great advantage of such circuits is that they can be found on a compact scale, which can be placed inside the drum part of the structure. The design and verification of those analog electric circuits are out of the scope of this paper.

The same procedure for designing the PPF controller which has been done for the numerical study is carried out for the experimental tests in this section. In order to select the best loop for each mode, it is required to extract the open-loop transfer functions first. For this purpose, an actuator of a pair excites the structure using a chirp signal within the frequency range of interest, i.e., 1100 Hz–1400 Hz, while the sensor voltage of the same pair is measured simultaneously. This test repeats for all pairs. The FRFs of the open-loop transfer functions for all pairs are shown in Fig. 13. Interestingly, the FRFs are all collocated containing alternating pole and zero. Moreover, five resonances can be identified in a short range of frequency. Therefore, the experimental FRFs are comparable to those of the numerical response shown in Fig. 8. The resonances are however in a slightly wider range of
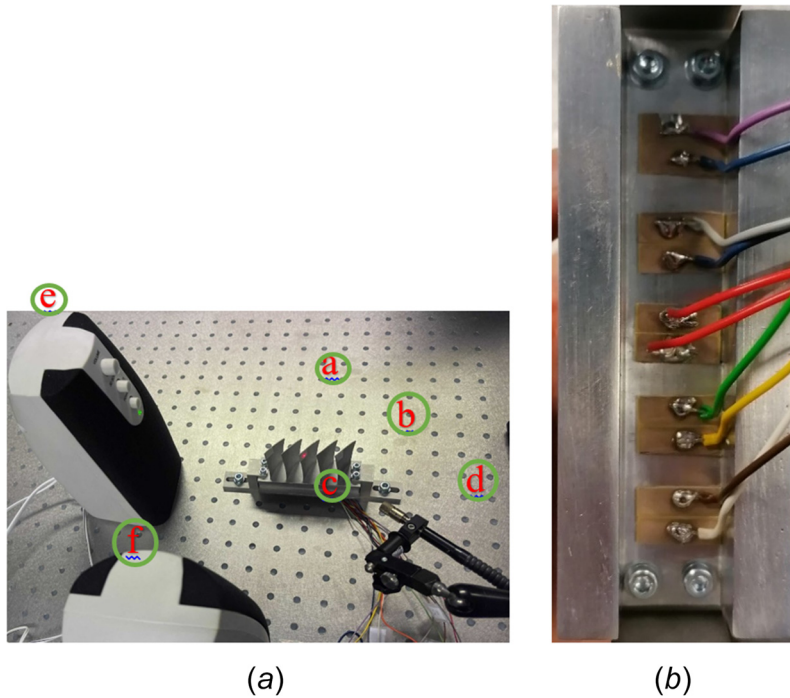
Fig. 12 (*a*) **Experimental setup of bladed rail with detail components:** (*a*) **bladed rail,** (*b*) **clamped support,** (*c*) **piezoelectric patches' cables,** (*d*) **laser vibrometer (measuring the middle blades displacement),** (*e*) **acoustic exciter no. 1, and** (*f*) **acoustic exciter no. 2 and** (*b*) **the piezoelectric patches mounted on the bladed rail**

frequency compared to the numerical resonances (Fig. 9). This is the effect of boundary conditions. In fact, the rigidity of the support will influence the separation of the resonances in a family. When the support is more rigid, the resonances of the family are placed more close to each other. This is the case for the numerical model as the ideal rigid boundary conditions have been considered. Using the same method which has been explained in Sec. 3 for selecting the best loop for each mode, the following configuration is selected: the third, the first, the fifth, the second, and the fourth loops target the first, the second, the third, the fourth, and the fifth modes, respectively.
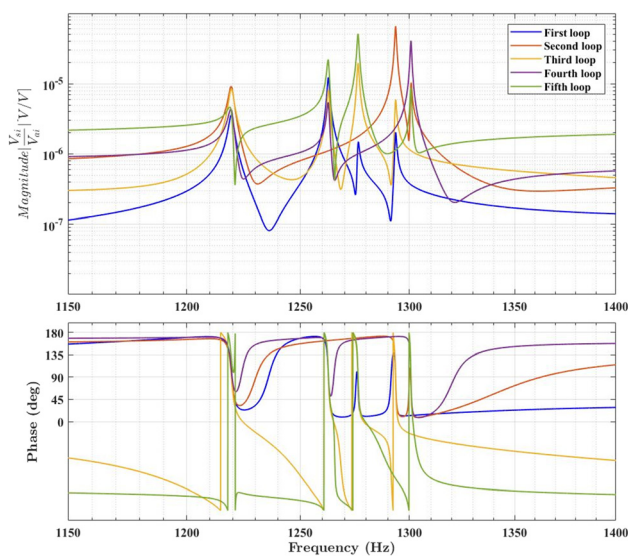
An optimal PPF can now be obtained for each loop using Eq. (2). Then, the performance of the designed control system for each loop is evaluated as a single input single output system. For this purpose, the FRFs of the experimental loop gain of each loop are shown in Fig. 14. It indicates how each controller is effective in a target mode. In addition, one sees that each control system ensures the stability of the closed-loop system. To understand the effective of a PPF on a target mode and other modes, the FRFs of the open-loop and the closed-loop responses of the first loops are presented in Fig. 15 as an example. One sees that the second mode is effectively damped. Also, the damping of the third and the fourth modes slightly increases.
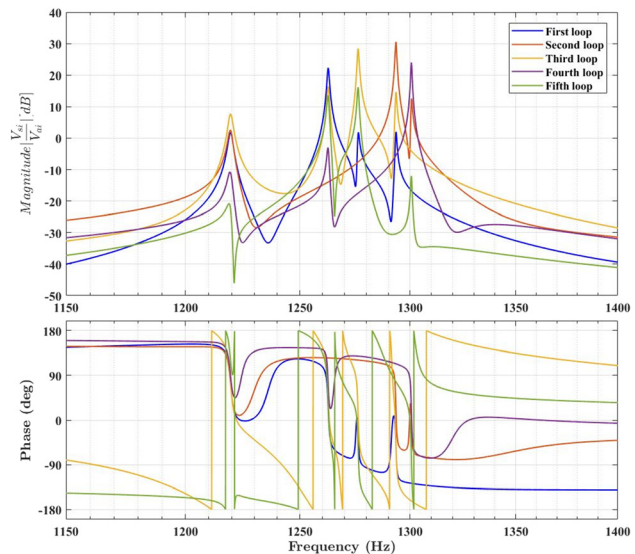

Fig. 13 Experimental FRFs of the open-loop transfer functions from each piezoelectric actuator to the collocated piezoelectric sensor for each loop

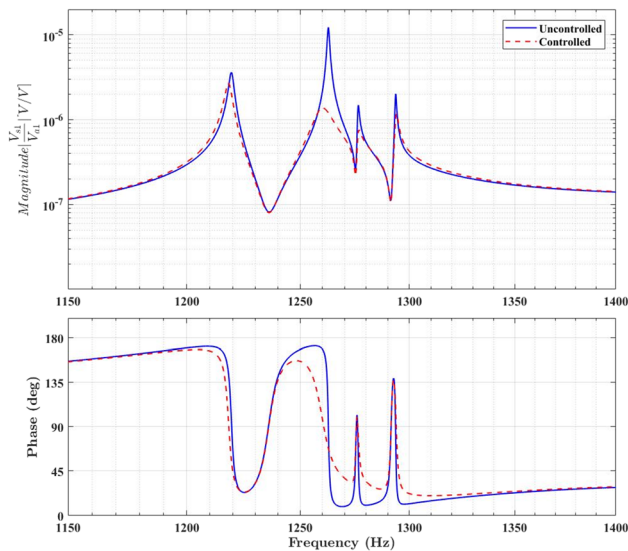**Fig. 14 Experimental FRFs of the loops gains**

Fig. 15 Open loop and closed loop response of loop no. 1 (experimental)

After designing a separate PPF controller for each loop, all of the loops are closed to evaluate the effectiveness of the decentralized multiple-input and multiple-output controller on the first family of mode experimentally. For this purpose, an acoustic excitation system is considered to excite the structure within the frequency range of 1150 Hz–1400 Hz. For measuring the output of the system, a laser vibrometer is used to measure the velocity of the middle blade's tip. In this arrangement, the performance index of the system is defined by the transfer function from the acoustic excitation signal to the laser vibrometer signal. For making sure that all of the five modes in the family of mode is excited, two speakers are placed in a perpendicular shape to excite the structure properly in different directions.

The FRFs of the performance index of the bladed rail with and without the decentralized control system is presented in Fig. 16. First, all of the modes in the first family mode can be observed in the uncontrolled response. In addition, the proposed decentralized PPF controller can mitigate effectively the vibration of the five modes in the first modes family. The first resonance is however
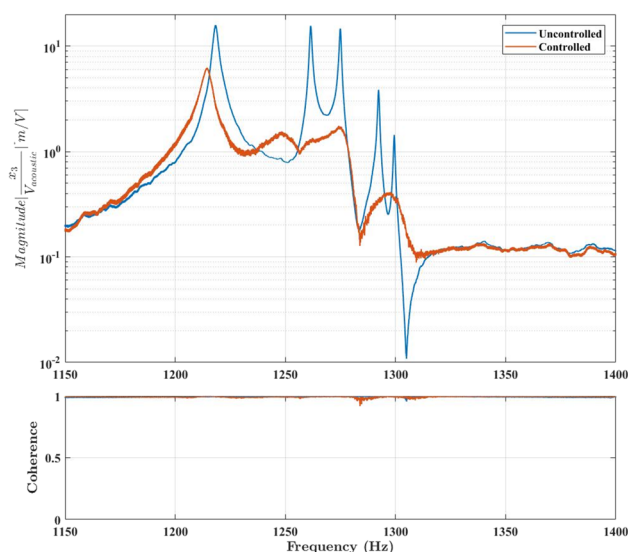
not significantly damped compared to other resonances. This is because each PPF has a positive impact in terms of damping on higher modes as shown in Figs. 15 and 10. Therefore, other than the PPF which targets the first resonance in the third loop, no other PPF almost adds damping to this mode.

As shown in Fig. 12, an acoustic system excites the structure in the frequency range of interest. It is needed to ensure that all the resonances of the first family are excited properly. For this purpose, the coherence of the signal with and without the control system is evaluated. The coherence is a statistic that indicates how much the output is correlated with the input in frequency domain. Mathematically, it is obtained from the cross spectral-density between input and output divided by the autospectral density of both input and output [24]. The value of one shows the most correlation and the value of zero indicates the least correlation. Figure 16 shows the coherence in the frequency range of excitation. It is almost one for both controlled and uncontrolled response. This means that there is a good correlation between the acoustic excitation and the measured response at the tip of the blade.

5 Conclusion

In this study, an active control system has been proposed to mitigate the resonances of the first family modes of the bladed structures. The control system has been implemented numerically and experimentally on a bladed rail structure. Piezoelectric patches have been used for both sensing the motion and actuating the control force. For obtaining maximum control authority, the size and location of piezoelectric patches have been optimized based on maximizing the strain energy. Although locating the patches at the blade root maximizes the strain energy, it results in important perturbations of the aerodynamic flow. Therefore, a pair of sensors and actuators is placed below the root of each blade inside the support. It has been shown that the pairs provide good control results due to alternating pole and zero pattern in the FRF and good controllability and observability. A decentralized PPF controller has been designed such that a PPF in a loop targets a certain mode of the family. Although the PPF as a second-order filter has been designed to damp one mode, it can be effective to damp multiple modes of a high modal density resonances system like a family of resonances of the bladed rail. The efficiency of the proposed control system has been validated experimentally on a manufactured bladed rail.

Fig. 16 The performance index of the bladed rail structure in uncontrolled and controlled conditions (all the loops are closed)

References

[1] Griffin, J. H., 1990, "A Review of Friction Damping of Turbine Blade Vibration," Int. J. Turbo Jet Engines, **7**(3–4), pp. 297–308.
[2] Laxalde, D., Gibert, C., and Thouverez, F., 2008, "Experimental and Numerical Investigations of Friction Rings Damping of Blisks," ASME Paper No. 43154.
[3] Laxalde, D., Thouverez, F., and Lombard, J.-P., 2010, "Forced Response Analysis of Integrally Bladed Disks With Friction Ring Dampers," ASME J. Vib. Acoust., **132**(1), p. 011013.
[4] Firrone, C. M., Allara, M., and Gola, M. M., 2008, "A Contact Model for Nonlinear Forced Response Prediction of Turbine Blades: Calculation Techniques and Experimental Comparison," ASME Paper No. GT2008-51231.
[5] Hagood, N. W., and von Flotow, A., 1991, "Damping of Structural Vibrations With Piezoelectric Materials and Passive Electrical Networks," J. Sound Vib., **146**(2), pp. 243–268.
[6] Schwarzendahl, S. M., Szwedowicz, J., Neubauer, M., Panning, L., and Wallaschek, J., 2012, "On Blade Damping Technology Using Passive Piezoelectric Dampers," ASME Paper No. GT2012-68600.
[7] Mokrani, B., Bastaits, R., Horodinca, M., Romanescu, I., Burda, I., Viguié, R., and Preumont, A., 2015, "Parallel Piezoelectric Shunt Damping of Rotationally Periodic Structures," Adv. Mater. Sci. Eng., **2015**, pp. 1–12.
[8] Forward, R. L., 1979, "Electromechanical Transducer-Coupled Mechanical Structure With Negative Capacitance Compensation Circuit," U.S. Patent No. 4,158,787.

[9] Preumont, A., 2011, *Vibration Control of Active Structures: An Introduction*, Vol. 179, Springer-Verlag Berlin Heidelberg.

[10] Kauffman, J., and Lesieutre, G., 2011, "Vibration Reduction of Turbomachinery Bladed Disks With Changing Dynamics Using Piezoelectric Materials," AIAA Paper No. 2011–2003.

[11] Hohl, A., Neubauer, M., Schwarzendahl, S., Panning, L., and Wallaschek, J., 2009, "Active and Semiactive Vibration Damping of Turbine Blades With Piezoceramics," Active and Passive Smart Structures and Integrated Systems, International Society for Optics and Photonics, Vol. 7288, San Diego, CA, p. 72881H.

[12] Tang, J., and Wang, K., 1999, "Vibration Control of Rotationally Periodic Structures Using Passive Piezoelectric Shunt Networks and Active Compensation," ASME J. Vib. Acoust., **121**(3), pp. 379–390.

[13] Agnes, G. S., 1994, "Active/Passive Piezoelectric Vibration Suppression," *Smart Materials and Structures 1994: Passive Damping*, Vol. 2193, International Society for Optics and Photonics, pp. 24–34.

[14] Duffy, K. P., Choi, B. B., Provenza, A. J., Min, J. B., and Kray, N., 2013, "Active Piezoelectric Vibration Control of Subscale Composite Fan Blades," ASME J. Eng. Gas Turbines Power, **135**(1), p. 011601.

[15] Simonich, J. C., 1994, "Actuator Feasibility Study for Active Control of Ducted Axial Fan Noise," NASA, Washington, DC, Report No. NASA-CR-195412.

[16] Sutliff, D., Hu, Z., Pla, F., Heidelberg, L., Sutliff, D., Hu, Z., Pla, F., and Heidelberg, L., 1996, "Active Noise Control of Low Speed Fan Rotor-Stator Modes," AIAA Paper No. 97–1641.

[17] Thomas, R. H., Burdisso, R. A., Fuller, C. R., and O'Brien, W. F., 1994, "Active Control of Fan Noise From a Turbofan Engine," AIAA J., **32**(1), pp. 23–30.

[18] Kousen, K. A., and Verdon, J. M., 1994, "Active Control of Wake/Blade-Row Interaction Noise," AIAA J., **32**(10), pp. 1953–1960.

[19] Remington, P., Sutliff, D., and Sommerfeldt, S., 2003, "Active Control of Low-Speed Fan Tonal Noise Using Actuators Mounted in Stator Vanes: Part 1 Control System Design and Implementation," American Institute of Aeronautics and Astronautics (AIAA), Reston, VA.

[20] Paknejad, A., Zhao, G., Osée, M., Deraemaeker, A., Robert, F., and Collette, C., 2020, "A Novel Design of Positive Position Feedback Controller Based on Maximum Damping and H_2 Optimization," J. Vib. Control, **26**(15–16).

[21] Zhao, G., Paknejad, A., Raze, G., Deraemaeker, A., Kerschen, G., and Collette, C., 2019, "Nonlinear Positive Position Feedback Control for Mitigation of Nonlinear Vibrations," Mech. Syst. Signal Process., **132**, pp. 457–470.

[22] Balmes, E., and Deraemaeker, A., 2013, "Modeling Structures With Piezoelectric Materials," SDT Tutorial, Paris, France.

[23] Balmes, E., Bianchi, J-P., and Leclere, J-M., 2010, "Structural Dynamics Toolbox FEMLink, Version 6.1" SDT Tutorial, Paris, France.

[24] Singiresu, S. R., 1995, *Mechanical Vibrations*, Addison Wesley, Boston, MA.